Fuel 353 (2023) 129136

Contents lists available at ScienceDirect

Fuel

journal homepage: www.elsevier.com/locate/fuel

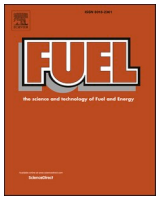

Full Length Article

Maximizing Sustainable aviation fuel usage through optimization of distillation cut points and blending

Zhibin Yang [a,*], Randall C. Boehm [a], David C. Bell [a], Joshua S. Heyne [a,b]

[a] Bioproduct, Sciences, and Engineering Laboratory, School of Engineering and Applied Science, Washington State University, Richland, WA 99354, USA
[b] Energy Processes and Materials Division, Energy and Environment Directorate, Pacific Northwest National Laboratory, Richland, WA 99352, USA

ARTICLE INFO

Keywords:
Distillation optimization
Sustainable aviation fuel
Muti-dimensional optimization
Pareto front
Conventional jet fuel

ABSTRACT

Sustainable aviation fuel pathways do not generally yield selective synthetic blend components in the aviation turbine fuel distillation range. Here we discuss a methodology for maximizing the sustainable aviation fuel yield from a pathway and the respective blend ratio with a petroleum-derived fuel by varying distillation cut points. These cut points are typically unique for each combination of feedstock and conversion technology and are essential independent variables for fuel finishing. The resultant cut point variations create a Pareto front, illuminating a competition between yield and blend ratio limits, i.e., the boundary where key operability properties are on the specification limit. Computational and experimental examples are given herein. In the computational case, eight bulk properties are calculated for a surrogate composition to simultaneously predict the competition between distillation yield and blend limit, with 10 points along the Pareto front experimentally verified. In the experimental optimization example, this methodology has been applied to an actual product stream currently under development. Relative to a third-party distillation cut recommendation, the method here yielded 37 %v more renewable carbon into the SAF fraction, while also affording a greater margin to property specification limits. This article shares the optimization process which can impact SAF qualification, the relative corresponding diesel and gasoline fractions, and business strategy.

1. Introduction

Sustainable aviation fuel (SAF) remains the principle strategy for the aviation industry to achieve net-zero carbon emissions by 2050 [1]. Alternative strategies include hydrogen combustion and electric motors powered by batteries or fuel cells. However, 73% of aviation CO_2 emissions come from medium and long-haul flights, which exceed the technology readiness levels expected for electric and hydrogen-powered aircraft capability over the next several decades [2–4]. To achieve the net zero 2050 goal, it is estimated that 330–445 million tons of SAF per annum are needed [1]. In theory, a multitude of production pathways will be developed and qualified in order to achieve this goal. This work is intended to serve that goal.

All synthetic aviation fuel production pathways (whether sustainable or not) must be qualified through a process described in ASTM D4054 [5]. Historically, all pathways were required to be considered for four tiers of testing, with the volumes required to eclipse the process ranging from 100 gallons to hundreds of thousands of gallons and years to complete. Under this process, pathways have been qualified for up to 50 %v blends with conventional fuels. More recently, another qualification path has emerged, fast track. The fast track approval requires 100 gallons of neat fuel, two tiers of testing, and ideally only one year to complete the evaluation, and may result in approval to use the SAF in blends with conventional fuel up to 10 %v. Production pathways that achieve fast track approval produce a fuel blend component with a narrower set of control specifications than those passing through the standard approval process. Either way, production pathways that receive a favorable review (and ballot) of the evaluation carried out under ASTM D4054 will be included as a new or edited annex in ASTM D7566 [6], which is the document describing the feedstock, process, and product specification limits for the synthetic pathway.

Prescreening has already demonstrated the ability to accelerate and de-risk SAF process and technology development [7–9]. Heyne et al. [10] proposed two levels of prescreening (requiring 1 to 5 ml and 150 to 500 ml of sample, respectively) focusing on properties that may influence flight safety [11,12]; density, viscosity, surface tension, derived cetane number (DCN), flash point, freeze point, and lower heating value (LHV). By identifying inconsistencies between the properties of candidate product streams and those of conventional jet fuel, qualification

* Corresponding author.
E-mail address: zhibin.yang@wsu.edu (Z. Yang).

https://doi.org/10.1016/j.fuel.2023.129136
Received 20 February 2023; Received in revised form 25 June 2023; Accepted 28 June 2023
Available online 12 July 2023

Nomenclature

B_F	Blended fraction - the fraction of SAF blended into conventional jet fuel; mass of SAF divided by mass of the conventional fuel plus mass of SAF.
D_F	Distilled fraction - mass collected as SAF after distillation divided by mass of the renewable product stream supplied to the still.
m_{acti}	Mass of actual i^{th} component in the renewable product stream
m_{opti}	Mass of optimized i^{th} component in the renewable product stream
y_i	Mass fraction of i^{th} component
API	American Petroleum Institute gravity
ASTM	ASTM International
CI	Confidence Interval
DCN	Derived Cetane Number
DMCO	1,4-dimethylcyclooctane
FID	Flame Ionization Detector
GCxGC	Two-Dimensional Gas Chromatography
JudO	Jet Fuel Blend Optimizer
LHV	Lower Heating Value
MIDACO	Mixed Integer Distributed Ant Colony Optimization
SAF	Sustainable Aviation Fuel
SIP	Synthesized Iso-Paraffins
VFA	Volatile Fatty Acids

risks (or other opportunities) can be highlighted while the scale-up process is readily and inexpensively adjustable. Moreover, project-management decisions concerning the prioritization of competing SAF technologies can be made with as much information as possible and as early as possible.

Conventional fuel blend components are also an importance consideration for blend limits and potentially SAF yield. In order for a SAF blend component to be used in an aircraft, it must be blended with an on spec conventional fuel (ASTM D1655) at a ratio no higher than the approved limits set in the annexes of ASTM D7566. Additionally, the blended SAF-conventional fuel must meet ASTM D7566 Table 1 and 2 properties for it to be regarded as a Jet A/A-1 (ASTM 1655). This process has many important considerations for an institution such as, the size and location of a blending facility, the SAF pathway in question, and properties of the initial conventional fuel to name a few. The property variance from conventional fuels can be substantial [12], and in turn, constrain SAF blend limits at a blending facility, which in turn can cascade to various financial impacts. The impacts of conventional fuel variance on SAF blending is yet to be explored in the literature.

Unlike conventional jet fuel, SAF may be very selective (e.g., Annex 3 SIP) or, in other cases, composed of a broad suite of hydrocarbon constituents, depending on its feedstock source and production process. For a selective process, most of the renewable carbon product stream should end up in the finished SAF, and distillation (if needed) can be considered a purification step. For non-selective processes, however, the product stream could contain species ranging from as few as five to many (>26) carbon atoms per molecule (distillation range, 36 to > 450 °C), which is broader than the jet fuel range. In these cases, distillation can be used to separate the product stream into fractions, where the monetary value of each fraction varies based on contemporary policies, and the properties of that fraction. While this is essentially the same process as petroleum refining, the population distribution of different molecular species with a given distillation cut could be markedly different depending on the pathway, and those composition differences result in significant property differences. In this work, property predictions of virtual distillation fractions blended at varied ratios with a nominal conventional Jet A are used to guide the optimal cut points for the distillation of the renewable carbon product stream.

Fuel production process optimization has long been an interest in the fuel community. Feedstock selection/pre-processing, conversion technology, and distillation all influence product yields. Miller et al. [13] explored the possibility of optimizing biomass upgrading strategies for transportation fuel based on maximum bio-blendstock content, applied to a case study with biomass-derived volatile fatty acids (VFA) for transportation fuels with the potential to extend to many non-VFA inputs. Zhang et al. [14] were able to improve the carbon yield of renewable alkanes for jet fuels from a feedstock selection and pre-processing perspective by co-feeding cellulose and low-density polyethylene. Peng et al. [15] explored the optimization of conversion technology (hydrocracking) to improve jet fuel yield and quality from vacuum gas oil, with hydrocracking already being a component of the Fischer-Tropsch SAF pathway (i.e., ASTM D7566 A1 and A4).

Most distillation optimization research, however, has been done on crude oil distillation and focused on industrial processes. For example, Franzoi et al. [16] explored the optimization of cut point temperature of crude oil distillation units to improve distillation yield and properties (i.e., sulfur content) toward a specific fraction (i.e., naphtha fraction). They used a surrogate modeling approach to estimate compositions and properties (API and sulfur) of distillates based on the existing data from a plant or rigorous simulated data. Lopez et al. [17] were able to develop a nonlinear programming model to simultaneously optimize crude oil blending and operating conditions of crude oil distillation units for maximum system profit (USD/day). None of these works address both SAF distillation yield and blend ratio with conventional jet fuels (i.e., Jet A), while predicting and measuring eight key operability properties as done here.

In this work, we report a methodology that leverages hydrocarbon composition input to illuminate the spectrum of solutions between maximum blend ratio and SAF yield. This method uses properties models to predict distillation cut points that maximize, simultaneously, distillation yield (the fraction of renewable carbon product stream that goes to yield SAF) and blend limit (the maximum ratio of the SAF fraction that can be blended into conventional jet fuel) by performing a two-objective, multi-constrained optimization. Convergence occurs when neither the yield nor blend limit can be improved without compromising the other, and the set of points meeting that condition is called the Pareto front. A high-level flow chart describing the optimization approach is shown in Fig. 1. To guide the optimization, the Jet Fuel Blend Optimizer platform (JudO) [18,19] was used to manage the constrained optimization, where fuel properties subject to spec limits were calculated from blending rules [19–23], a molecular property database [24], and trial product composition derived from the objective functions. For experimental validation of this optimization, two validation methods are reported. First, simple blends mimicking the optimization results were prepared and blended with Jet A (POSF 10325) until a property limit was violated. A second validation was completed by simulating the path taken by the JudO simulation. There an initial mixture was prepared in the lab, and cut points from the JudO simulation were used to experimentally acquire trial SAF fractions. Subsequently, those SAF fractions were blended with Jet A at ± 2 %v increments until a property limit was violated, as in the first validation case.

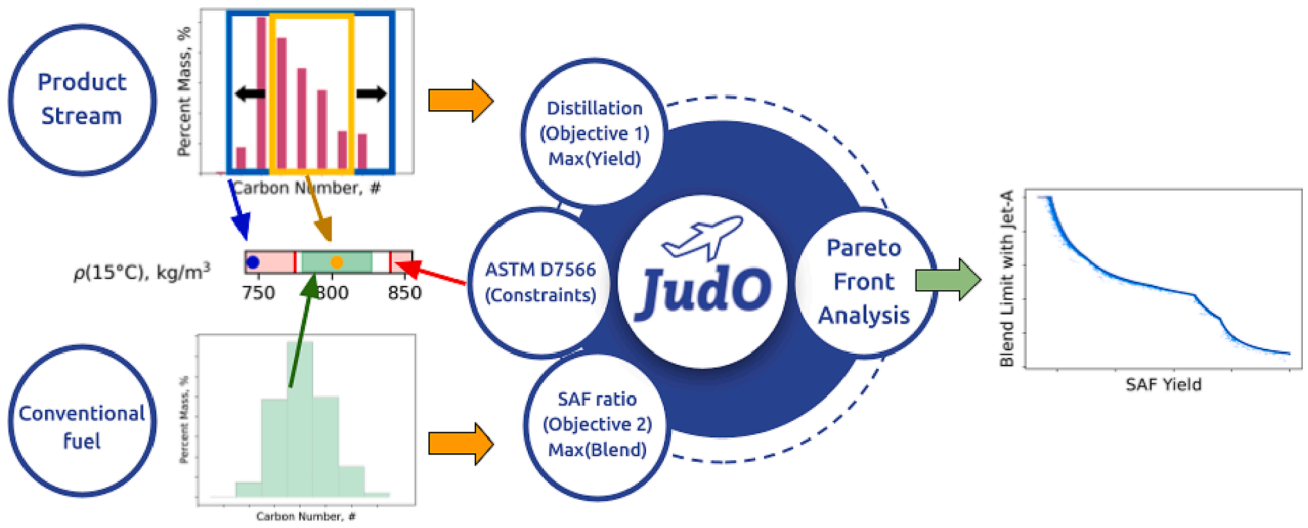

Fig. 1. Flow chart of the methodology reported here. Distillation simulation, property predictions, and blend limit with conventional jet fuel are calculated simultaneously within the JudO optimization software to meet the ASTM D7566 property requirement. The resulting Pareto front represents a set of optimal solutions.

The process described here could be easily adapted to other scenarios, and an experimental method mimicking the computational example above is also reported. For that part of the study, the optimal distillation cut of a product stream for an actual, prospective production pathway was guided by the method reported in this work. The result of this method is then compared to those of a third party working from the same sample product stream. Our approach enabled significantly higher SAF yield (37% more volume) and a greater margin to property spec limits. Beyond increasing the SAF yield, this methodology illuminates the entire scope of potential routes a producer could pursue for qualification or business strategy.

2. Experimental methods

2.1. Material

Six hydrocarbon materials were sourced from five vendors to create a surrogate renewable carbon product stream. The intention of this surrogate is not meant to mimic conventional jet fuels but rather to create an arbitrary product stream. The materials and their compositions were selected primarily based on the ability to represent an arbitrary product stream that fails to meet spec for a plurality of reasons (i.e., out of spec flash point, freezing point, and density, etc.). Additional considerations included availability, cost, and purity. The petroleum fuel is represented here by a nominal Jet A (A-2 [POSF 10325]). The details of the materials used for the mixture are provided in Table 1.

2.2. Gas chromatography method

Two-dimensional gas chromatography (GCxGC) coupled with a flame ionization detector (FID) was used to determine species concentrations of distilled mixtures, as described by Heyne et al. [25]. The GC × GC system employed an Agilent 8890 with a SepSolve INSIGHT flow modulator. The columns are arranged in a reverse configuration with an Rxi-17Sil MS 60 m × 0.32 mm × 0.5 μm first-dimension column from Restek and an Rxi-1 ms 15 m × 0.32 mm × 0.5 μm second dimension column, also from Restek. The carrier gas is grade 5.0 helium with flows of 1.2 ml/min and 48 ml/min through the first and second dimension columns, respectively. The temperature profile of the GC starts at 40 °C for 30 s and increases by 1 °C/min until 280 °C.

2.3. Fractional distillation

Fractional distillation was utilized in this study to perform distillation cuts on the surrogate product stream that fails to meet spec. The benchtop distillation unit setup consists of a 125 ml flat bottom boiling flask connected to a Synthware Jacketed Vigreux Distillation Head (Synthware D214300), and a receiving graduated cylinder. A thermometer is inserted through the top of the jacketed Vigreux column per ASTM D86 guidance; a picture of the setup is provided in the supplementary information. The hot plate temperature is increased periodically to achieve a consistent receiving rate of 1 ml/min. Boiling stones are also used to increase efficiency and consistency. The average time from the first application of heat to the initial boiling point is five

Table 1
Hydrocarbons used in the surrogate renewable carbon product stream, including blend ratios and suppliers.

Material name	Purity	Supplier	Blended mass fraction
2,2,4-trimethylpentane	>99%	Sigma-Aldrich	0.2398
n-octane	99%	ACROS	0.2086
n-nonane	99%	ACROS	0.1777
1,4-dimethylcyclooctane	98.5%	B.G. Harvey, NAWCWD and M. Karanjikar, Clean Joule	0.0811
n-decane	99%	thermo scientific	0.1807
n-tridecane	>99%	TCI	0.1121

Table 2
Fuel property measurement and equipment used in this study, along with the associated ASTM methods (if available).

Property	Company/model	ASTM or other methods
Density, viscosity	Anton Paar – SVM 3001	D7042
Freezing point	PAC – Phase FPA-70Xi	D5972
Flash point	PAC – OptiFlash	D3828
†DCN	Tier Alpha/GC	Ref [27]
Surface tension	CSC – DuNouy Tensiometers	D1331A
Smoke point	Koehler- Smoke Point Lamp	D1322
†LHV	Tier Alpha/GC	Ref [21]

†These properties were estimated from blending rules only. The rest were measured in accordance with the procedures described in the applicable ASTM test method as called out in ASTM D7566.

minutes. The total volume supplied and collected is recorded during each run, which forms the basis for the distillation yield. Three fractional distillations, each employing different cut points, were carried out for this study. None of the distillations were replicated, so no comment regarding the repeatability of the yield fraction composition can be made. A fractional distillation unit is used instead of a traditional D86 setup due to the high separation efficiency needed in this study. The Vigreux distillation head is generally accepted to have 6–8 theoretical plates, depending on the heating rate and geometry [26].

2.4. Property measurement

Each fuel property that affects engine operability was measured according to its respective ASTM method as documented in D7566 (Table 2). Other properties, including DCN and LHV, were determined from the blending rules only, due to the high cost of the samples, the sample volume required for DCN measurement, and in case of the LHV, the exceptional accuracy of the blending rule methodology [21]. Measurement for all individual properties at any given time was measured once according to the ASTM method and reported reproducibility is used later as uncertainty quantification.

2.5. Maximum blend fraction determination by experimentation

A stepwise method is used to determine the maximum blend limit of each distillation cut with the conventional jet fuel, A-2. An initial (trial) blend fraction is selected based on guidance from the simulation. Each property, listed in Table 2, of the trial fuel was determined. If one or more properties were outside of spec limits, a new blend fraction containing 2 %v less SAF was tested, and this step was repeated until an acceptable blend fraction was found. If all the properties of the initial trial fuel were determined to be within spec, then a new blend fraction containing 2 %v more SAF was tested, and this step was repeated until an unacceptable blend fraction was found. The 2 %v step size was motivated by the repeatability of each property determination and the time required to characterize each trial fuel.

3. Computational methods

3.1. Overview

The optimization in this study is based on two objectives: 1) the fraction of renewable carbon to be used as SAF; mass collected as SAF after distillation divided by mass of the renewable product stream supplied to the still (D_F) and 2) the fraction of SAF blended into conventional jet fuel; mass of SAF divided by mass of the conventional fuel plus mass of SAF (B_F). In a perfect scenario here, the SAF fraction would have a 100 % yield and be 100% drop-in (max D_F and B_F), i.e., no blending with Jet A required. Here all the circular carbon would be used and that carbon would not need any conventional or fossil carbon to complement it to be fungible. In reality, there are no pathways with this capability. Instead, as documented herein there is a compromise between renewable carbon and the associated blend limits.

3.2. Approximations and assumptions

The mixture used here to represent a renewable carbon product stream contains six compounds, all of which are known. For a real fuel, composition is determined through GCxGC hydrocarbon type analysis, where species are characterized by number of carbons atoms and principle skeletal features such as chains, rings, aromaticity, etc. The precise isomer corresponding to each peak on a chromatogram would have to be represented as a distribution of possible isomers as described by Yang et al. [27]. Secondly, the virtual distillation done for each trial in the optimization routine assumes complete separation by normal boiling point (i.e., infinite theoretical plates). In reality the number of theoretical plates is a function of the temperature gradient within the still between the mixture and the distillate, the effective area of nucleation sites throughout the fractionating column and the transport rate of liquid away from the fractionating column. While the still used in this work has estimated 6–8 theoretical plates, the components of the surrogate have disparate boiling points, rendering it easy to separate cleanly back into its components via distillation. Finally, only continuous range distillation cuts were considered in this work. In reality, it is possible that some renewable carbon product streams could be very high in certain aromatic compounds or certain normal alkanes, with challenging properties. These property challenges could, for example, cause a trial fuel to fail on smoke point or freeze point if left alone. In those cases, discontinuous range or fractional distillation cuts could be considered as an extension to this fundamental idea.

3.3. Objectives and constraints / blending rules

Nine constraints on fuel properties were imposed on every trial fuel in the simulation, where one of them is an equality constraint and rest of them are inequality constraints (indicated in Table 3). The specification limit constraints are listed in Table 3 and were motivated by their impact on combustor operability. The determination of trial fuel properties was made by application of blending rules as described in a variety of publications [20–23,28]. Additionally, the mass factions must always sum to one and it is only possible to remove mass from either end of distillation range. Mass can never be added, and no mass can be removed until it is found at the end of the distillation range. Where m_{opti} is the mass of

Table 3
Optimization parameters used in JudO.

Objectives	Physical or logical constraints	Spec limit constraints	
$\max(D_F)$	$0 \le m_{opti} \le m_{acti}$	Density(15 °C): 775 – 840 Kg/m3	Derived cetane number: 35 – 60
$\max(B_F)$	$^{*}\sum y_i = 1$	Viscosity(-20 °C): <8 cStViscosity (-40 °C): <12 cSt Freezing point < -40 °C Flash point: > 38 °C	Surface tension, report Smoke point: > 18 mm Lower heating value (LHV): > 42.8 MJ/kg

* This constraint is an equality constraint.

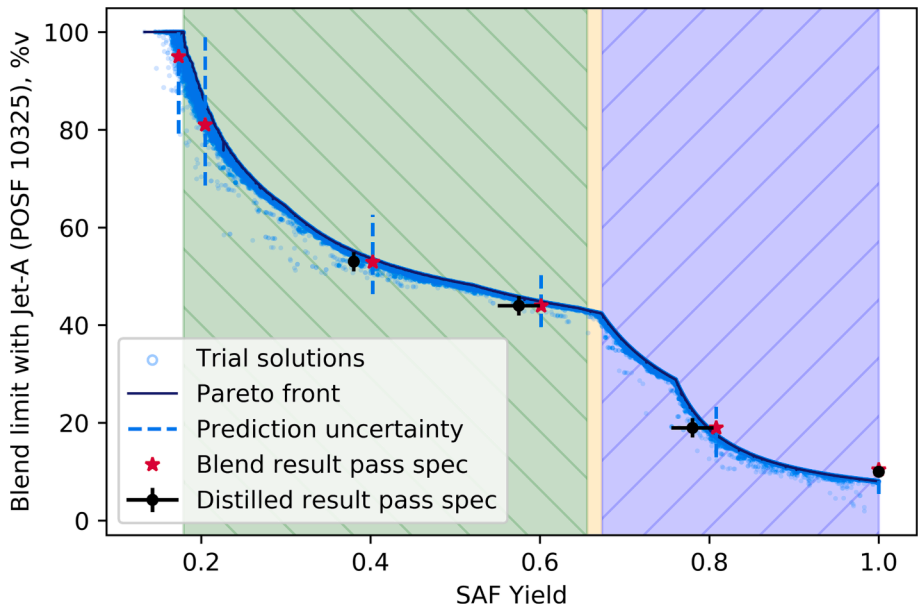

Fig. 2. Pareto front from the muti-dimensional optimization of the surrogate product stream described in Table 2. The blue, yellow, and green shaded region represents blends limited by flash point, density, both density and freeze point, respectively. Two types of experimental validation of the Pareto front are shown in black and red markers. (For interpretation of the references to colour in this figure legend, the reader is referred to the web version of this article.)

optimized ith component in the renewable product stream and m_{acti} is the mass of actual ith component in the renewable product stream. The sum of all m_{opti} equals D_F; mass collected as SAF after distillation divided by mass of the renewable product stream supplied to the still.

3.4. Convergence criteria

Optimization convergence was declared when 3,000 consecutive iterations failed to find a solution with ($\geq B_F$ AND $\geq D_F$) relative to at least one other point on the evolving Pareto front or ($>B_F$ OR $> D_F$) relative to all other points on the evolving Pareto front. More detail on this convergence criteria was reported by Schlueter [29].

3.5. Software tools

The optimization tool developed here is built on the framework of Jet Fuel Blend Optimizer (JudO) from previous works [18,30]. A commercially available mixed integer distributed ant colony optimization (MIDACO) [31] is utilized in JudO as the numerical solver due to its robustness and computational time. MIDACO is based on a derivative-free, evolutionary hybrid algorithm employing n-dimensional random walk. This algorithm treats the objective and constraint functions as black-box which may contain critical function properties like non-linearity, non-convexity, discontinuities or even stochastic noise. This solver has been used in several fuel-related optimization applications [18,30,32].

3.6. Uncertainty quantification

For simulated points, the 95th percentile confidence intervals arise from the composite of limiting properties prediction uncertainty where the prediction uncertainty includes 3 (or 4) terms: unidentified isomer (e.g. compounds originating from the conventional fuel), uncertain mass fraction which is relatively small, uncertain component property input, and uncertain blending rule accuracy is applied to the property predictions. Monte Carlo sampling is used for uncertainty quantification because it is effective for tracing isomeric uncertainty and for convenience it was used across the board; 10,000 points in all. For more detail regarding related Monte Carlo sampling on uncertainty, see Heyne et. al. and Yang et. al. [25,27].

For experimental points, the 95th percentile confidence intervals arise from the property measurement uncertainty and mass measurement (SAF yield) uncertainties corresponding to the retained distillation fraction and the original mass of the surrogate product stream.

4. Results & discussion

The optimization of the initial blend described in Table 1 was performed on a 32-core processor with a base clock speed of 3.7 GHz. Convergence was achieved after 24 h. Fig. 2 reports these results. 154,410 trial solutions are reported (light open circles), of which approximately ten percent (15,736) are found on the Pareto front (solid blue line). The uncertainty of the property and thus Pareto front predictions are also reported (vertical blue dashed lines). The predictions ranged from 8 %v and 100% SAF yield to a 100 %v blend limit and 18% SAF yield. Three types of properties limits occurred during the optimization, which were flash point constraint (blue shaded region), density constraint (yellow shaded region), and both density and freeze point constraints (green shaded region). Four apparent inflection points on the Pareto front were observed, with the inflection points being the result of discrete changes to the limiting constraint(s) or to the species being cut from the SAF fraction.

Inspecting from right to left of Fig. 2, at 100% SAF yield or the uncut mixture, the blend limit with A-2 (POSF 10325) is 8 %v. In other words, 8% is the maximum amount of renewable carbon that can be blended into A-2 before some specification limit is violated. Even though the mixture described in Table 2 fails the spec limit on multiple grounds (i.e., flash point, density, etc.), all of these violations are eliminated by mixing with 92 %v or more nominal petroleum jet fuel, A-2. As less desirable species were removed from the mixture by distillation, the distilled mixture property was closer to the spec range and the SAF blend limit with A-2 naturally increased as well. At 18 %v SAF distillation yield, most undesired molecules were removed by distillation of the original mixture. The distilled mixture meets the spec requirements and thus no petroleum fuel is required.

Experimental validations of these predictions are reported for the blended (red star) and distilled (black circles) cases. The uncertainty associated with property measurement (solid black vertical lines) and

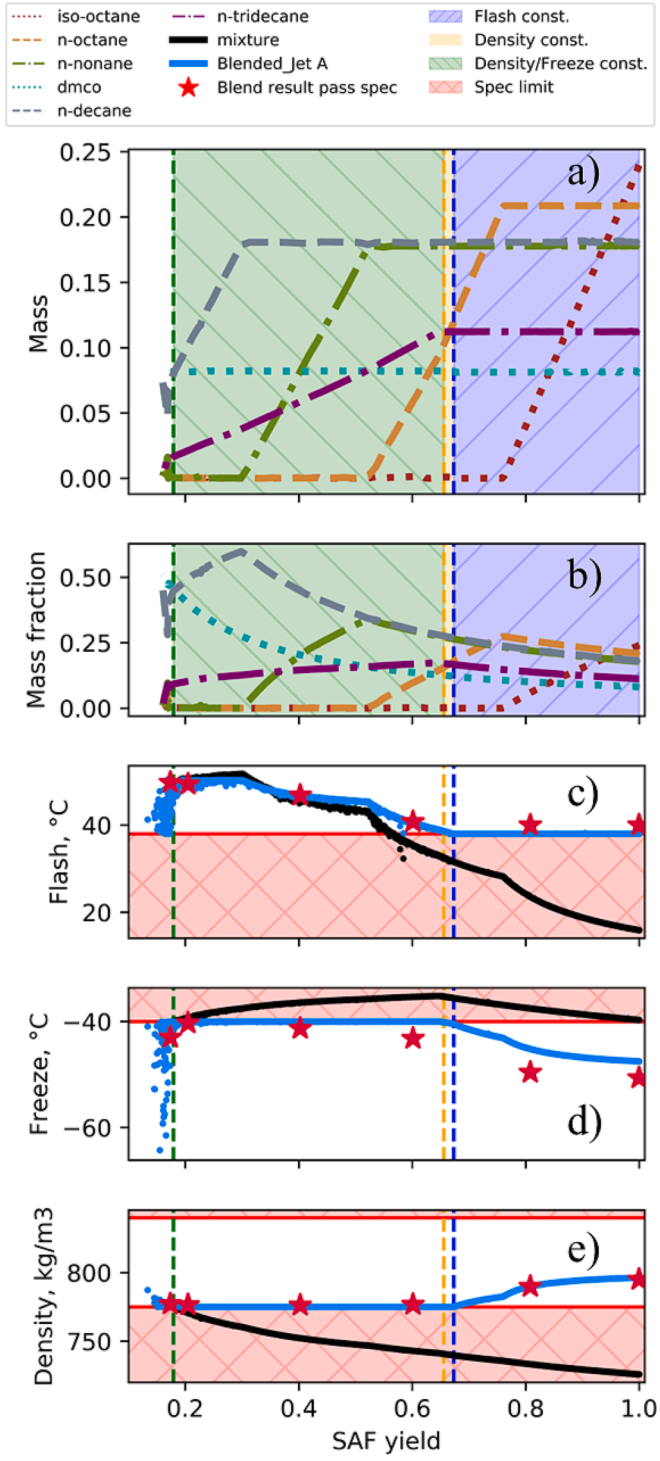

Fig. 3. Composition and property of the calculated Pareto Front in Fig. 2. a & b) mass and mass fraction of each surrogate component described in Table 2. c, d, & e) limiting properties of the SAF fraction and blended product.

SAF yield determination (solid black horizontal lines) are also reported. Validation consists of two parts: the Pareto front determination and the impact of infinite plate assumption. Six mixtures, mimicking perfectly separated distillation cuts, are prepared by blending Table 1 individual components in the lab. Additionally, three separate real distillations were carried out on the surrogate product stream described in Table 1, resulting in three separate distillation cuts as well as the uncut surrogate product stream. The total volume supplied and collected were recorded during each run, which forms the basis for the distillation yield. In some cases, the collected volume is the distillate, and in other cases it is the bottom fraction. In each case, a characterization via GCxGC/FID was completed for both the collected (prospective fuel blend component) and discarded fraction to determine the mass fraction of each component (documented in SI). As for the mixtures prepared by blending Table 1 components, the volumes used were recorded for the uncertainty analysis later.

The six mixtures made by blending were utilized for validation of the Pareto front determination. The maximum blend ratio of these mixtures with A-2 (POSF 10325) was determined by trial and error, as described in the methods section. The difference between the predicted blend limit (solid blue line) and the measured blend limit (red stars) represents modeling error. This is compared against known modeling uncertainty and measurement uncertainty by the 95th percentile confidence intervals. The modeling error across six points were 2.3 %v on average, and the biggest error occurred at 100 %v blend limit, which is 5 %v.

The three mixtures made by fractional distillation (black circles) were used to assess the impact of the infinite plate assumption. The differences between the black circles to the closest solid blue line and red stars to the closest solid blue line represent the error introduced by the infinite plates assumption. The larger error is due to the unnecessary species being removed from the mixture during the physical distillation. Naturally, the distilled test results are below the calculated Pareto front because the Pareto front represents the theoretical maximum. The considerable uncertainty in SAF distillation yield indicated by two of the three points is a consequence of our indirect determination of the retained fraction of renewable carbon. This method required estimation of the dynamic hold-up (dead volume) in two cases since the mass of the bottom fraction was not measured directly. The dead volume was later determined empirically for this setup. No attempt to minimize dead volume relative to feed volume was made for this study, although certainly, it could be reduced substantially for a production-quality still or refinery.

Fig. 3 reports the composition and properties variation along the Pareto front. In all sub-plots, the x-axis is the SAF fraction distillation yield. In descending order vertically, Fig. 3a and 3b represent the mass and mass fraction (colored circles), respectively, of each SAF mixture component along the Pareto front. On Fig. 3c, 3d and 3e, the property of

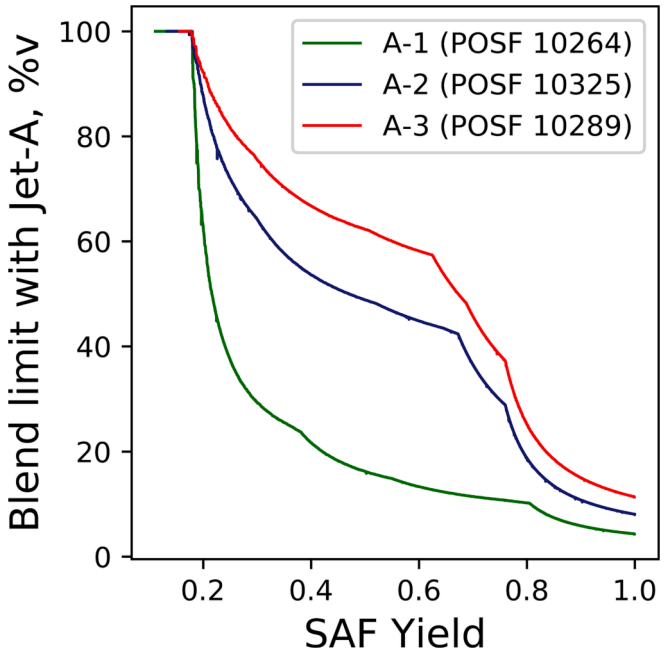

Fig. 4. Pareto fronts of reference conventional jet fuels to illustrate the jet fuel variance effect on SAF blend limit.

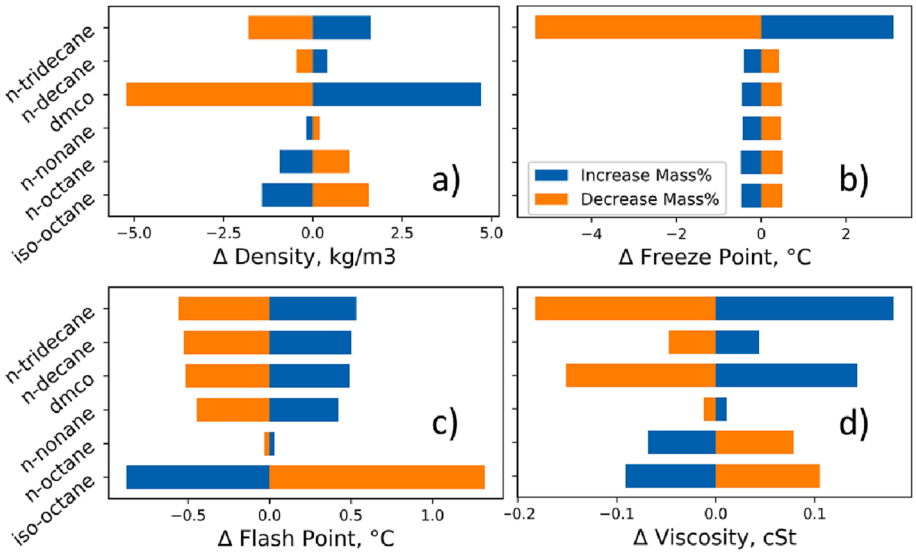

Fig. 5. Sensitivity analysis of fuel surrogate described in Table 1.

the distilled SAF fraction (solid black lines) and final product, after blending with A-2 (solid blue lines) are reported. The three types of property limits (colored shaded region and lines) reported in Fig. 2 are also plotted in Fig. 3 for reference. Finally, the properties of the six blends used for model validation (red stars) are also reported here.

At a SAF yield of 66.5% and higher the limiting property is flash point. This is evident in Fig. 3c which shows the SAF fraction has a flash point lower than the specified minimum while the SAF-conventional blend has a flash point right on the spec limit of 38 °C. From Fig. 3a and 3b it is clear that *iso*-octane and n-octane are the two components that contribute most to the violation of flash point. As more of these components are removed, the flash point of the prospective SAF increases, enabling more of it to be blended into A-2. The change in curvature of black line on Fig. 3c corresponds to the change in the identity of the component being removed (*iso*-octane vs n-octane). Flash point is driven by the sum of the components' vapor pressures which all scale exponentially with the inverse of the normal boiling point. Therefore, the component with the lowest boiling point disproportionately affects the flash point of the mixture. Moreover, flash point decreases more sharply with declining n-octane concentration than some other properties, such as density. These trends are responsible for the emergence of density as a limiting property for SAF yield fractions below 66.5% (Fig. 3a and 3e). In the narrow band between the dashed yellow and blue lines, density is the only limiting property as incrementally more n-octane is removed from the SAF fraction. At 66% SAF yield fraction and below, freeze point is also limiting, driven by the concentration of n-tridecane in the final product, as shown Fig. 3a and 3d. Even more dramatically than flash point, the freeze point is driven by the concentration of one (or few) species; usually those having the highest normal melting point [23]. In this case, n-tridecane also has the highest boiling point of the components in this mixture, enabling the optimizer to remove it, together with n-octane, the current lowest boiling point component. This is important to manage density which is driven lower by the removal of n-tridecane and higher by the removal of n-octane. At still lower SAF yield fraction, n-octane is depleted, and density lost by removing n-tridecane must be managed by removing other light components such as n-nonane and n-decane. The only component of the surrogate SAF product stream that is not removed by the optimizer is 1,4-dimethylcyclooctane (DMCO). This is because all of its key operability properties lie within the jet fuel spec range. Other properties, not considered for this work, such 8% aromatics minimum, T90-T10 and T50-T10 would ultimately limit the maximum allowable concentration of any single molecule, including DMCO for a commercially viable SAF product.

Thus far, only the variance of the distillation cut points of the SAF fraction have been discussed in comparison to nominal jet fuel, A-2 (POSF 10325). Here we illustrate the importance of the conventional or fossil component in these calculations with two additional conventional fuels (A-1 [POSF 10264] and A-3 [POSF 10289]) in Fig. 4. Similar to Fig. 2, A-1 and A-3 generated two additional Pareto fronts. Those fuels were selected by the National Jet Fuel Combustion Program to represent the 'best' and 'worst' conventional jet fuels, considering then-anticipated fuel property impacts on combustor operability [12]. The greatest difference in blend limit between A-1(solid green line) and A-3 (solid red line) occurs at 63% SAF yield, where there was a 44 %v difference in blend limit with different conventional fuels. To achieve a 50% blend limit with each fuel, the difference of SAF yield can range from 22% (A-1) to 67% (A-3). The limiting properties to achieve a higher blend ratio with A-1 were flash point, flash point with density, density, and density with freeze point from descending order of 100% SAF yield. For blends with A-3 the limiting properties were flash point, flash point with freeze point, and freeze point with density. All three reference fuels have relatively the same freeze point (i.e., −50 to −51 °C). The distance between each line on the Pareto front is mostly caused by the density and flash point difference of A-1 (i.e., 780 kg/m^3, 42 °C) and A-3 (i.e., 827 kg/m^3, 60 °C).

The curvature and order of the Pareto fronts would also change if the product streams were different, which further suggests value in doing an optimization like this for each grouping of available blend stocks; SAF product stream(s) and petroleum fuel(s).

In our experience as a lab dedicated to assisting SAF development and evaluations, four competing properties usually determine the Pareto front: flash point, viscosity, density, and freeze point. Where flash point violation is predominately caused by the light end and freeze point violation is predominately caused by one or more of the higher melting point molecules (typically C13 + n-alkanes) [33]. Density and viscosity are functions of both the light end and heavy end combined. Removing light end to fix flash point drives up all of the other properties, pushing freeze point or viscosity or both above targets and removing heavy end to fix freeze point drives down all of the other properties, pushing flash point or density or both below targets. All issues need to be fixed in concert.

To illustrate how each property is influenced by selecting the SAF composition a sensitivity analysis was performed on the uncut mixture using Tier alpha [27] models, and its results are summarized in Fig. 5. A set of 13 calculations was made for each property. One of those

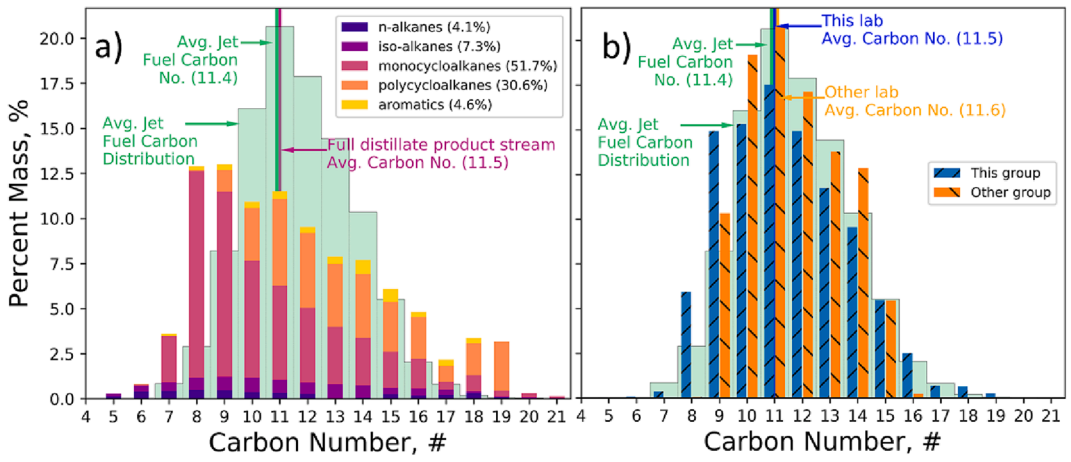

Fig. 6. A) carbon distribution of the full product stream from anonymous fuel producer. b) carbon distribution of two different distillation cut on the same full distillate fuel, for simplicity only the summed carbon group is shown.

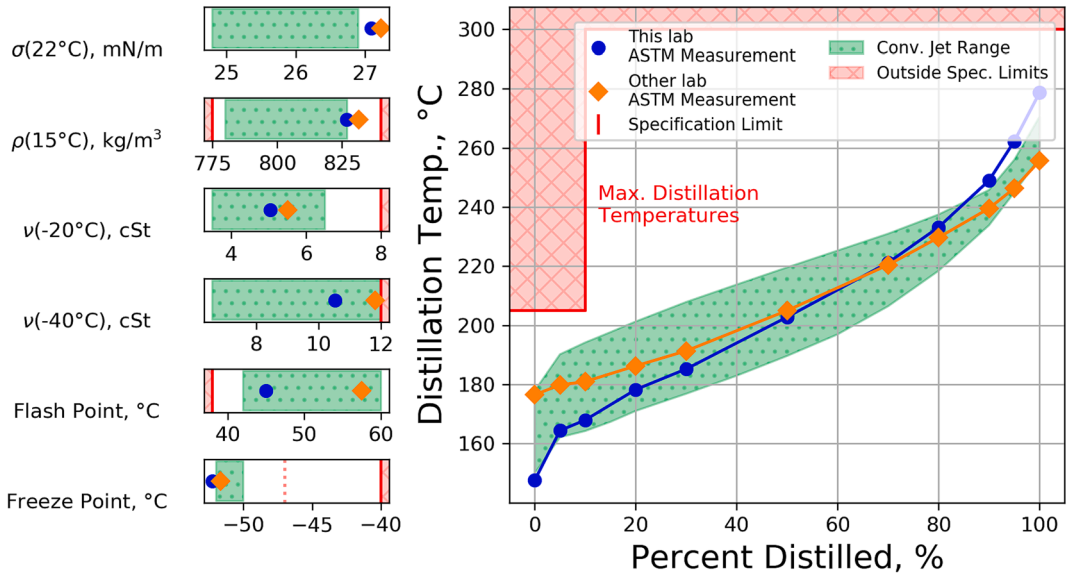

Fig. 7. A) tier beta critical property measurements comparison of two different distillation cuts. b) d86 correlation distillation curve for two cuts. the tighter distillation cut of the 'other lab' resulted in properties worse than the wider cut for viscosity, density, surface tension, and freeze point.

corresponds with the surrogate product stream composition. Starting from 100 g of that composition in each case 5 g of, sequentially, each component was added or subtracted to form the virtual mixtures corresponding with the other 12 calculations. Density (a) is symmetric about zero since it is very nearly linear with mass fraction. A change in DMCO concentration has the largest impact on mixture density because its density (824 kg/m^3) is furthest from that of the original mixture (726 kg/m^3). The freeze point (b) is determined by the mole fraction and properties of tridecane; non-linearly with negative curvature over the full range of possible mole fractions [23]. Removing 5 g of n-tridecane impacts the freeze point significantly more than adding 5 g. Adding or removing any other component from the mixture impacts freeze point because the tridecane mole fraction varies as the total mass of the other components vary. Flash point (c) is a little more complex than freeze point as two components contribute significantly to the vapor pressure, *iso*-octane and n-octane. Coincidentally, the vapor pressure of *iso*-octane is nearly 5 times higher than the vapor pressure of n-octane so adding or subtracting 5 g of n-octane has approximately the opposite effect on the total mixture vapor pressure as increasing or decreasing the concentration of *iso*-octane by 1%. When any of the other components are removed from the mixture, its total vapor pressure increases because the concentration of both isomers of octane increase. Removing *iso*-octane has a larger influence on flash point than adding it because the second derivative of vapor pressure with temperature is positive. Viscosity (d) also has a non-linear blending rule so some asymmetry about zero is expected and seen. Like density, changing the concentration of species who's neat, log viscosity value are further from that of the baseline mixture have more impact on the final result than changing the concentration of species who's neat, log property value are closer to that of the baseline mixture.

5. Practical application and discussion

A renewable carbon product stream from a novel process was recently delivered to two labs, including ours for processing into SAF. As per the procedure described above, we determined the optimal distillation cut should be 155–270 °C to maximize the SAF yield. The other lab took a narrower cut (est. 176–255 °C based on ASTM D2887 result), presumably to be conservative relative to property limits. Naturally, our cut resulted in a higher conversion yield and it also, unintuitively, resulted in a product with a greater margin to property limits. Fig. 6a is the detailed carbon distribution from GCxGC hydrocarbon type analysis

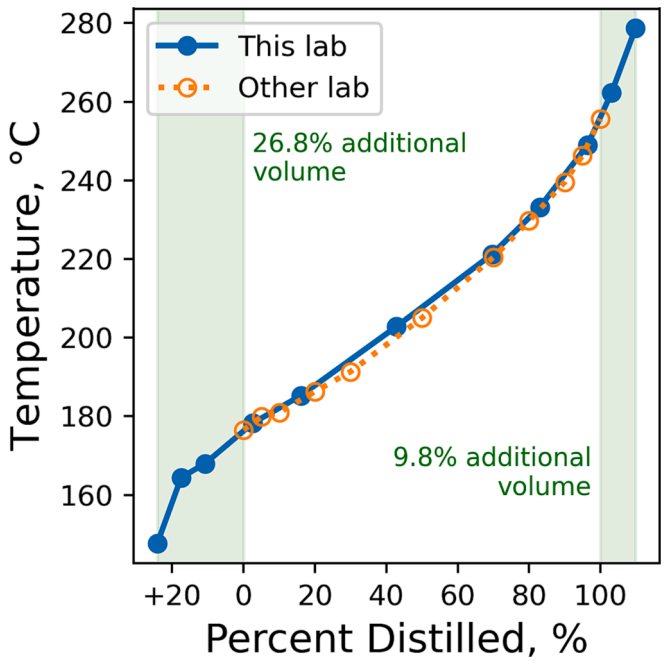

Fig. 8. Distillation recovery comparison of two different cuts on the same full distillate fuel.

of the renewable carbon product stream. It included compounds with 5–21 carbon atoms. Several key properties (flash point, viscosity, freeze point) of the renewable carbon product stream fell outside of spec. Fig. 6b is the carbon distribution of the two SAF cuts from the two different labs but with the same hydrocarbon type analysis method and experimental set up. Note that the other lab achieved crisper separation between the components, as our still was set to match ASTM D86, which achieves essentially one theoretical plate, the minimum. Also note that we retained compounds with 7–19 carbon atoms while other lab retained compounds with 9–16 carbon atoms. Both distillation cuts and the product stream had similar average carbon numbers, 11.5 versus 11.6. However, the kinematic viscosity at −40 °C of the SAF fraction from the other lab was measured to be 11.8 cSt, compared to a spec limit maximum of 12.0 cSt. By comparison, the viscosity of the SAF fraction from this lab was 9.8 cSt. The reason for this difference is that viscosity is reduced more by the addition of 18.3 % of light compounds than it is decreased by the reduction of a similar fraction of heavy compounds, analogous to the sensitivity results summarized in Fig. 5. Additional property comparisons between the two samples are provided in Fig. 7. Of the properties measured, our SAF sample is closer to the spec limit only with respect to flash point.

Last, we investigate the SAF yield for both distillation cuts. In this step, we match the IBP and FBP of the other lab's distillation curve temperatures to interpolated values from our lab's distillation temperatures. Then, our lab's result is rescaled, broadening the percent distilled beyond the values of 0 to 100 % recovered. Fig. 8 illustrates the result of this process. Where the narrower distillation curve (i.e., other lab) is not changed, the broader cut (i.e., this lab) is scaled to match the same exact temperature on the narrow curve, which results in an estimated volume difference. The missing 26.8% volume in the light end is from cutting out the C7, C8, and some portion of C9 as shown in Fig. 6b. The 9.8% volume in the heavy end is mostly contributed from C16, C17, and C18. Combined, this lab utilized 36.6 %v more renewable carbon in the SAF fraction than the other lab and the properties that are most important for combustor operability are objectively better. It should be noted that this exercise here did not consider other fuel properties that are also important for approval process (i.e., thermal stability). In practice, the final neat product and potential blends would be experimentally tested.

It is worth noting that the overlapping portion of distillation curve match well, as expected, since they both started with the same renewable carbon product stream, which validates our scaling methodology.

6. Conclusion

A novel methodology was discussed here for maximizing the sustainable aviation fuel yield from a pathway and the respective blend ratio with conventional jet fuel by varying distillation cut points. This optimization considers eight bulk properties simultaneously to predict the competition of SAF yield and blend limit with conventional jet fuel. This methodology was then applied to both a surrogate and an applied practical case. In the surrogate case, ten points along the optimization generated Pareto front were experimentally validated, from which good agreement was observed. As for the practical application of this methodology, this approach achieved 37% more renewable carbon into SAF fraction and affording greater margin to spec limit compared to a third party. Conventional jet fuel variance effect on the blend limit was also investigated, which also has great influence on the blend limit. This paper functions as proof of concept that a renewable carbon product stream can be optimized based on the maximum SAF fraction yield and maximum blend ratio with Jet A. Eventually this tool should extend the capability to both renewable gasoline and diesel fractions and be able to incorporate TEA LCA, and contemporary policies for a well to wake analysis of different fraction of full range product stream (gasoline, SAF, diesel).

Declaration of Competing Interest

The authors declare that they have no known competing financial interests or personal relationships that could have appeared to influence the work reported in this paper.

Data availability

Data will be made available on request.

Acknowledgements

The authors would like to acknowledge funding from the U.S. Federal Aviation Administration Office of Environment and Energy through ASCENT, the FAA Center of Excellence for Alternative Jet Fuels and the Environment, project 65 through FAA Awards 13-CAJFE-UD-026 and 13-CAJFE-WASU-035 (PI: Dr. Joshua Heyne) under the supervision of Dr. Anna Oldani. Any opinions, findings, conclusions, or recommendations expressed in this material are those of the authors and do not necessarily reflect the views of the FAA or other sponsors.

Appendix A. Supplementary data

Supplementary data to this article can be found online at https://doi.org/10.1016/j.fuel.2023.129136.

References

[1] Air Transport Action Group. WAYPOINT 2050. 2021.
[2] Collins JM, McLarty D. All-electric commercial aviation with solid oxide fuel cell-gas turbine-battery hybrids. Appl Energy 2020;265:114787. https://doi.org/10.1016/J.APENERGY.2020.114787.
[3] Nicolay S, Karpuk S, Liu Y, Elham A. Conceptual design and optimization of a general aviation aircraft with fuel cells and hydrogen. Int J Hydrogen Energy 2021;46:32676–94. https://doi.org/10.1016/J.IJHYDENE.2021.07.127.
[4] Ng KS, Farooq D, Yang A. Global biorenewable development strategies for sustainable aviation fuel production. Renew Sustain Energy Rev 2021;150:111502. https://doi.org/10.1016/J.RSER.2021.111502.
[5] West Conshohocken 2022. https://doi.org/10.1520/D4054-22.
[6] Astm. D7566: Standard Specification for Aviation Turbine Fuel Containing Synthesized Hydrocarbons. West Conshohocken 2020. https://doi.org/10.1520/D7566-22A.

[7] Huq NA, Hafenstine GR, Huo X, Nguyen H, Tifft SM, Conklin DR, et al. Toward net-zero sustainable aviation fuel with wet waste–derived volatile fatty acids. Proc Natl Acad Sci USA 2021;118(13).
[8] Yang Z, Xu Z, Feng M, Cort JR, Gieleciak R, Heyne J, et al. Lignin-based jet fuel and its blending effect with conventional jet fuel. Fuel 2022;321. https://doi.org/10.1016/j.fuel.2022.124040.
[9] Stone ML, Webber MS, Mounfield WP, Bell DC, Christensen E, Morais ARC, et al. Continuous hydrodeoxygenation of lignin to jet-range aromatic hydrocarbons. Article Continuous hydrodeoxygenation of lignin to jet-range aromatic hydrocarbons Continuous hydrodeoxygenation of lignin to jet-range aromatic hydrocarbons 2022;6(10):2324–37.
[10] Heyne J, Rauch B, Le Clercq P, Colket M. Sustainable aviation fuel prescreening tools and procedures. Fuel 2021;290:120004. https://doi.org/10.1016/J.FUEL.2020.120004.
[11] Colket M, Heyne J, Rumizen M, Gupta M, Edwards T, Roquemore WM, et al. Overview of the National Jet Fuels Combustion Program. AIAA J 2017;55(4):1087–104.
[12] Fuel Effects on Operability of Aircraft Gas Turbine Combustors. Fuel Eff Operability Aircr Gas Turbine Combustors 2021. doi:10.2514/4.106040.
[13] Miller JH, Tifft SM, Wiatrowski MR, Benavides PT, Huq NA, Christensen ED, et al. Screening and evaluation of biomass upgrading strategies for sustainable transportation fuel production with biomass-derived volatile fatty acids. IScience 2022;25(11). https://doi.org/10.1016/j.isci.2022.105384.
[14] Zhang X, Lei H, Zhu L, Zhu X, Qian M, Yadavalli G, et al. Optimizing carbon efficiency of jet fuel range alkanes from cellulose co-fed with polyethylene via catalytically combined processes. Bioresour Technol 2016;214:45–54.
[15] Peng C, Cao Z, Du Y, Zeng R, Guo R, Duan X, et al. Optimization of a Pilot Hydrocracking Unit to Improve the Yield and Quality of Jet Fuel Together with Heavy Naphtha and Tail Oil. Ind Eng Chem Res 2018;57(6):2068–74.
[16] Gut JAW, Franzoi RE, Menezes BC, Kelly JD, Grossmann IE. Cutpoint temperature surrogate modeling for distillation yields and properties. Ind Eng Chem Res 2020;59:18616–28. https://doi.org/10.1021/acs.iecr.0c02868.
[17] López DC, Hoyos LJ, Mahecha CA, Arellano-Garcia H, Wozny G. Optimization model of crude oil distillation units for optimal crude oil blending and operating conditions. Ind Eng Chem Res 2013;52:12993–3005. https://doi.org/10.1021/ie4000344.
[18] Yang Z, Stachler R, Heyne JS. Orthogonal reference surrogate fuels for operability testing. Energies 2020;13:1–13. https://doi.org/10.3390/en13081948.
[19] Kosir S, Stachler R, Heyne J, Hauck F. High-performance jet fuel optimization and uncertainty analysis. Fuel 2020;281:118718. https://doi.org/10.1016/J.FUEL.2020.118718.
[20] Boehm RC, Hauck F, Yang Z, Wanstall CT, Heyne JS. Error quanti fi cation of the Arrhenius blending rule for viscosity of hydrocarbon mixtures 2022:1–15. https://doi.org/10.3389/fenrg.2022.1074699.
[21] Boehm RC, Yang Z, Bell DC, Feldhausen J, Heyne JS. Lower heating value of jet fuel from hydrocarbon class concentration data and thermo-chemical reference data: An uncertainty quantification. Fuel 2022;311:122542.
[22] Boehm RC, Yang Z, Heyne JS. Threshold Sooting Index of Sustainable Aviation Fuel Candidates from Composition Input Alone: Progress toward Uncertainty Quantification. Energy Fuel 2022;36(4):1916–28.
[23] Boehm RC, Coburn AA, Yang Z, Wanstall CT, Heyne JS. Blend Prediction Model for the Freeze Point of Jet Fuel Range Hydrocarbons. Blend Prediction Model for the Freeze Point of Jet Fuel Range Hydrocarbons 2022;36(19):12046–53.
[24] Kroenlein KG, Muzny CD, Diky V, Chirico RD, Magee JW, Abdulagatov IM, et al. NIST/TRC Web Thermo Tables (WTT) NIST Standard Reference Subscription Database 2 - Lite Edition Version 2 n.d.
[25] Heyne J, Bell D, Feldhausen J, Yang Z, Boehm R. Towards fuel composition and properties from Two-dimensional gas chromatography with flame ionization and vacuum ultraviolet spectroscopy. Fuel 2022;312:122709. https://doi.org/10.1016/j.fuel.2021.122709.
[26] Vigneault A, Johnson DK, Chornet E. Base-catalyzed depolymerization of lignin: Separation of monomers. Can J Chem Eng 2007;85:906–16. https://doi.org/10.1002/CJCE.5450850612.
[27] Yang Z, Kosir S, Stachler R, Shafer L, Anderson C, Heyne JS. A GC × GC Tier α combustor operability prescreening method for sustainable aviation fuel candidates. Fuel 2021;292:120345. https://doi.org/10.1016/j.fuel.2021.120345.
[28] Kosir ST, Behnke L, Heyne JS, Zabarnick S, Flora G, Denney RK, et al. Improvement in Jet Aircraft Operation with the Use of High-Performance Alternative Drop-in Fuels in Conventional Fuels. AIAA SciTech. Forum 2019:1–27.
[29] Schlueter M. MIDACO-SOLVER 2018. http://www.midaco-solver.com/.
[30] Kosir S, Heyne J, Kirby M. High-Performance Jet Fuel Optimization and Aircraft Performance Analysis Considering O-ring Volume Swell 2018:1–6.
[31] Schlueter M, Erb SO, Gerdts M, Kemble S. MIDACO on MINLP Space Applications n.d.:1–25.
[32] Behnke L, Monroe E, Nguyen B, Landera A, George A, Yang Z, et al. Maximizing net fuel economy improvement from fusel alcohol blends in gasoline using multivariate optimization. Fuel Commun 2022;11. https://doi.org/10.1016/j.jfueco.2022.100059.
[33] Link F, De Klerk A. Viscosity and Density of Narrow Distillation Cuts from Refined Petroleum- and Synthetic-Derived Distillates in the -60 to +60 °c Range. Energy Fuel 2022;36:12563–79. https://doi.org/10.1021/acs.energyfuels.2c02625.